TIME-LAPSE SEISMIC MODELING: ACCURACY REQUIRED TO DETECT SIGNALS FROM A WATERFLOODED RESERVOIR

A.R. SHAHIN*, P.L. STOFFA, R.H. TATHAM and R. SEIF

Jackson School of Geosciences, The University of Texas at Austin, Austin, TX 78713, U.S.A.
** Present address: BP Subsurface Technology, Reservoir Geophysics R&D, 501 West Lake Park Blvd., Houston, TX 77079, U.S.A. alireza.shahin@bp.com*

(Received May 1, 2011; revised version accepted November 18, 2011)

ABSTRACT

Shahin, A.R., Stoffa, P.L., Tatham, R.H. and Seif, R., 2012. Time-lapse seismic modeling: accuracy required to detect signals from a waterflooded reservoir. *Journal of Seismic Exploration*, 21: 49-82.

This paper investigates the ability of different seismic modeling techniques to detect changes in reservoir properties due to waterflooding into an oil reservoir. To do so, we simulate a poorly consolidated shaly sandstone reservoir model based on a prograding near-shore depositional environment. To account for the spatial distribution of petrophysical properties, an effective porosity model is first simulated by Gaussian geostatistics. Dispersed clay and dual water models are then efficiently combined with other well-known petrophysical correlations to consistently simulate the reservoir properties.

Next, the constructed reservoir model is subjected to numerical simulation of multi-phase fluid flow to predict the spatial distributions of pore pressure and water saturation due to water injection.

A geologically consistent stress-sensitive rock physics model, followed with modified Gassmann fluid substitution for shaly sandstones, is then utilized to simulate the seismic elastic parameters. Here, we insert the petro-elastic model into a one-dimensional background elastic model simulating the surrounding offshore sedimentary basin in which the reservoir was embedded. Finally, we employ different seismic modeling algorithms: one-dimensional (1D) acoustic and elastic ray tracing, 1D full elastic reflectivity, 2D split-step Fourier plane-wave (SFPW), and 2D stagger grid explicit finite difference, to simulate seismic waves propagated through the model and recorded at sea level. A base and two monitor surveys associated with 5 and 10 years of waterflooding are selected and the corresponding time-lapse signatures are analyzed at different incident angles.

0963-0651/12/$5.00

Our analyses demonstrate that internal multiples behind the waterfront, flooded zones, partially subtract out in time-lapse differencing, so they are less significant in monitoring projects than that of reservoir characterization.

We find that for time-lapse seismic modeling, acoustic modeling of an elastic medium is a good approximation up to ray parameter (p) equal to 0.2 s/km or surface incident angle of 17 degrees. But, at p = 0.3 s/km (surface incident angle of 27 degrees), difference between elastic and acoustic wave propagation is the most dominant effect other than internal multiples and converted waves. Here, converted waves are generated with significant amplitudes compared to primaries and internal multiples.

We also show that time-lapse modeling of the reservoir using SFPW approach is computationally fast compared to FD, 100 times faster for our case here. It is capable of handling higher frequencies than FD. It provides an accurate image of the waterflooding process comparable to FD. Consequently, it is a powerful alternative for time-lapse seismic modeling.

KEY WORDS: seismic, time-lapse, modeling, accuracy, waterflooding.

INTRODUCTION

In reservoir characterization, seismic reflectivity data have been extensively used to infer lithology and fluid characterization of subsurface rocks. More recently, time-lapse seismic surveying, repeated seismic surveys recorded at different calendar times over a depleting reservoir, is becoming one the most interesting applications for reservoir monitoring. The primary goal of time-lapse survey is to detect, estimate, and discriminate the changes in subsurface rock and fluid properties and ultimately to indentify flood fronts, preferential pathways, thief zones, and flow barriers, by-passed pay and infill targets.

In seismic reservoir monitoring, detecting small changes in seismic traveltimes and amplitudes is the key to successfully imaging the changes in reservoir properties. Seismic data as recorded are not just composed of primary arrivals with elastic reflection coefficients: also included will be internal multiples, converted waves, diffractions, etc. The question for this study, are these other arrivals significant enough to interfere with an analysis based solely on primary reflection coefficients. In responding to this question, here we briefly explain the current state of seismic modeling as a fundamental tool to investigate the effect of changes in reservoir properties on seismic data.

Seismic modeling simulates the propagation of elastic waves in a specified medium. Application of seismic modeling in exploration seismology can be categorized into four main areas including seismic survey design and illumination studies, seismic data processing, interpretation, and inversion. In different applications and for the sake of simplicity, seismologists approximate inelastic, heterogeneous, anisotropic, and 3D earth models with much more simpler models in dimension, e.g., 2D and 1D, and in properties, e.g., elastic, isotropic, and homogeneous.

There are several seismic modeling algorithms in seismology and they can be classified from various points of view. Accuracy, speed, and the range of wave phenomena that one seismic modeling algorithm can model, e.g., primary reflectors, multiples, converted waves, diffractions, head waves, critical reflections, etc., are some of the important factors in classifying seismic modeling approaches.

Currently, analytical, numerical, approximate, and hybrid seismic modeling algorithms are routinely used in academic and industrial projects. Here we summarize these methods.

Approximate seismic modeling methods

Ray theory is the cornerstone of many of the approximate methods. This theory consists of three fundamental parts including kinematic ray tracing, dynamic ray tracing, and polarization theory. Kinematic ray tracing describes the geometry and traveltimes of rays and wavefronts and it is governed by Snell's law. Dynamic ray tracing describes the geometrical spreading of rays and displacement magnitude. Finally, polarization theory describes the reflection and transmission coefficients, i.e., displacement direction, associated with interfaces in media (Chapman, 2004). In approximate seismic modeling methods, these theories will be combined to simulate the propagation of elastic high-frequency, body waves or 'rays' approximately instead of solving the exact wave equation analytically or numerically. These methods are all well-proved to be computationally efficient and faster than most purely numerical methods, e.g., finite difference and finite element methods. One other salient features of the approximate method is their ability to isolate elementary waves, e.g., specific arrivals of reflected P-and S-waves, multiples, etc., can be identified on synthetic seismograms. Nevertheless, they suffer from a lack of amplitude reliability when dealing with rapid changes in properties of the earth model. This is due to the fact that their formal validity criteria might be violated in complex geological models, e.g., sub-salt, gas cloud geology, and highly complex reservoir models of interest in time-lapse studies (Gjøystdal et al., 2007). Many other approaches have been proposed to overcome these difficulties by extending the standard ray theory: asymptotic or iterative ray theory, Maslov asymptotic ray theory, Quasi-isotropic ray theory, Born-scattering, Kirchhoff surface integral, Gaussian beam method (Červený, 1982; Hill, 1999), plane wave modeling (Stoffa et al., 2006). See Červený (2001) and Chapman (2004) for more references.

Analytical seismic modeling methods

Analytical methods solve the wave equations exactly for homogeneous and

one-dimensional (1D) stratified media. In these methods, transformation of the wave equation is performed to reduce the partial differential equation to a set of first-order ordinary differential equations, solved using a propagator matrix method. The computation of propagator matrices generates a synthetic seismogram in a transformed domain, i.e., frequency-horizontal ray parameter. Finally, inverse transformation over ray parameter and frequency leads to the wavefield response of the stratified medium in the time-offset domain [see Kennett (1985) and Chapman (2004) for more detail]. These algorithms are theoretically exact for 1D media because the multiples and mode-converted events are modeled.

Direct or numerical seismic modeling methods

To simulate the seismic response for an elastic complex earth model, one

Hybrid seismic modeling methods

Considering all the benefits and restrictions of these three seismic modeling (approximate, analytical, and numerical) methods, the next logical approach would be a hybrid approach providing fast and flexible modeling to handle complex geological models and having enough accuracy to be employed in seismic reservoir characterization and monitoring work flows.

Many papers address this concept for time-lapse seismic modeling by simulating a single seismic modeling for the overburden and conducting a set of repeated computations of seismic waveforms at the reservoir zone aimed at simulating the corresponding base and monitor surveys. Lecomte (1996), Gjøystdal et al. (1998), and Hùkstad et al. (1998) combined ray tracing in the overburden with repeated FD seismic modeling in the reservoir zone. Robertson and Chapman (2000) deployed a similar approach by applying FD seismic modeling in both the overburden and target to allow for strongly scattering heterogeneities of the entire model. Kirchner and Shapiro (2001) used FD to simulate wave propagation in the overburden and employed Born perturbation theory to compute the production-induced changes in time-lapse seismograms.

Here, we employ a recently-developed petro-elastic model [Shahin et al., 2010a for details] and use seismic modeling techniques with different degrees of accuracy, including: 1D acoustic with and without internal multiples, 1D elastic without internal multiples, 1D full elastic reflectivity, SFPW (described below) and staggered grid explicit FD. Next, we investigate the reservoir-scale effects of internal multiples, acoustic vs. elastic, the effect of converted waves, dimension of wave propagation (2D vs. 1D), and diffractions on time-lapse signatures. In addition, we demonstrate that the time-lapse response simulated with SFPW is closely correlated with the FD response but considerably faster to compute. Having superior speed to FD, the ability to model higher frequencies than FD, and yet comparable with FD and better than standard ray-based modeling, SFPW is the preferred method for reservoir characterization and monitoring workflows.

CONSTRUCTING A SYNTHETIC PETRO-ELASTIC RESERVOIR MODEL

Geological reservoir model

A stacked sand-rich strandplain reservoir architecture has been considered in this study to simulate a realistic geological framework. Strandplains are mainly marine-dominated depositional systems generated by seaward accretion of successive, parallel beach ridges welded onto the subaerial coastal mainlands. They are inherently progradational features and present on wave-dominated microtidal coasts (Tyler and Ambrose, 1986; Galloway and Hobday, 1996).

This sand-rich beach-ridge reservoir architecture is intended to be originally deposited as a clay-free geobody. However; due to post-depositional diagenesis, dispersed clay is produced and it is the main factor reducing porosity and permeability of the reservoir. This model, called SPE comparative solution project, is a large geostatistical model widely used in research on upgridding and upscaling approaches (Christie and Blunt, 2001). We select the top 35 layers of the model which is representative of the Tarbert formation, a part of the Brent sequence of middle Jurassic age and one of the major producers in North Sea. Next, we will assign geologically consistent petrophysics information and add facies characterization to develop a more realistic reservoir 2D model comparable to complicated models in the petroleum industry. The model is described on a regular Cartesian grid. The model size is $220 * 35$ in X (east-west) and Z (depth) directions, respectively. The grid size is $10 * 10$ meters, so the model dimensions are 2200 m by 350 m.

Petrophysics model

The geological model described above is used as the basic model in which petrophysical properties are populated assuming a meaningful petrophysics model. Here, the effective porosity model is first generated using Gaussian geostatistics and shale content and total porosity models are then computed assuming a dispersed clay distribution (Thomas and Stieber 1975; Marion et al. 1992). Permeability is calculated based on the extension of the dispersed clay model introduced by Revil and Cathles (1999). Next, we should initialize the reservoir for water saturation and pore pressure. An experimental correlation (Uden et al., 2004; Spikes et al., 2007) between water saturation and shale content is combined with the dual water model (Best 1980; Dewan, 1983; Clavier, 1984) to compute clay bound water, effective water saturation, total water saturation, and oil saturation. Initial reservoir pore pressure is simulated assuming a linear hydrostatic gradient from the top to the reservoir bottom.

Reservoir simulation

Fluid flow simulation combines three fundamental laws governing fluid motions in porous media. These laws are based on conservation of mass, momentum, and energy (Aziz and Settari, 1976). In this research, a commercial finite difference reservoir simulator, Eclipse 100, is utilized to replicate a waterflood enhanced oil recovery on a black-oil 2D reservoir containing oil, soluble gas, and water. The reservoir has no water drive. In addition, because of the high pressure conditions no gas is produced in the reservoir. Thus, prior to waterflooding solution gas is the only drive mechanism forcing oil to be produced. This drive is so weak that implementation of water injection is required to enhance oil recovery.

The same grid block dimensions used to generate the geological model, i.e., 10 by 10 square meters, are used to simulate fluid flow and seismic modeling; hence mathematical upscaling and/or downscaling was not necessary. For a period of 10 years, the waterflood schedule is simulated by using two injectors at the corners and one producer in the middle of the reservoir. In this period, saturations and pressures values for each reservoir grid block are exported after each year. Collecting this database allows us to analyze the sensitivity of the corresponding seismic data to a wide range of changes in fluid saturation and pressure.

Rock and fluid physics model

Rock and fluid physics modeling is the link between quantitative seismic interpretation, geology, and reservoir petrophysics. Using rock physics modeling, one can transform the petrophysical properties of a reservoir to seismic elastic parameters (Avseth et al., 2005) which can be further used to simulate seismic reflectivity data.

Combining the Dvorkin-Gutierrez rock physics model (2002), with the fluid physics model (Batzle and Wang, 1992), and using a modified Gassmann theory (Dvorkin et al., 2007), we were able to observe the joint effects of various petrophysical properties on elastic seismic parameters including P- and S-wave velocities, and density. Consequently, the comprehensive petro-elastic model can be efficiently utilized in sensitivity analysis of seismic data to changes in reservoir properties due to production (see Shahin et al., 2010a) for details and further applications of the petro-elastic model).

Fig. 1 shows the distribution time-lapse normalized percentage changes in effective water saturation, pore pressure, and the associated changes in seismic acoustic impedance (AI), and shear impedance (SI) between different base and monitor survey. Here, changes in elastic parameters, saturation, and pressure for the base survey (before waterflooding) are subtracted from those of the monitor survey (after waterflooding) and then normalized using those of the base survey, i.e., $\Delta\alpha = [(\alpha_{monitor} - \alpha_{base})/\alpha_{base}] * 100$, where α denotes any elastic or petrophysical parameter.

The corresponding petro-electric model for the reservoir can be efficiently simulated by combining the Thomas and Stieber petrophysics model (1975), dual water rock physics model (Best, 1980; Dewan, 1983; Clavier, 1984), and Arps' empirical equation (Arps, 1953). The joint modeling of the elastic and electrical properties of reservoir rocks will lead to the consistent forward modeling algorithms for joint inversion of seismic and electromagnetic (EM) data (see Shahin et al. (2010b) for further applications of the petro-electric model).

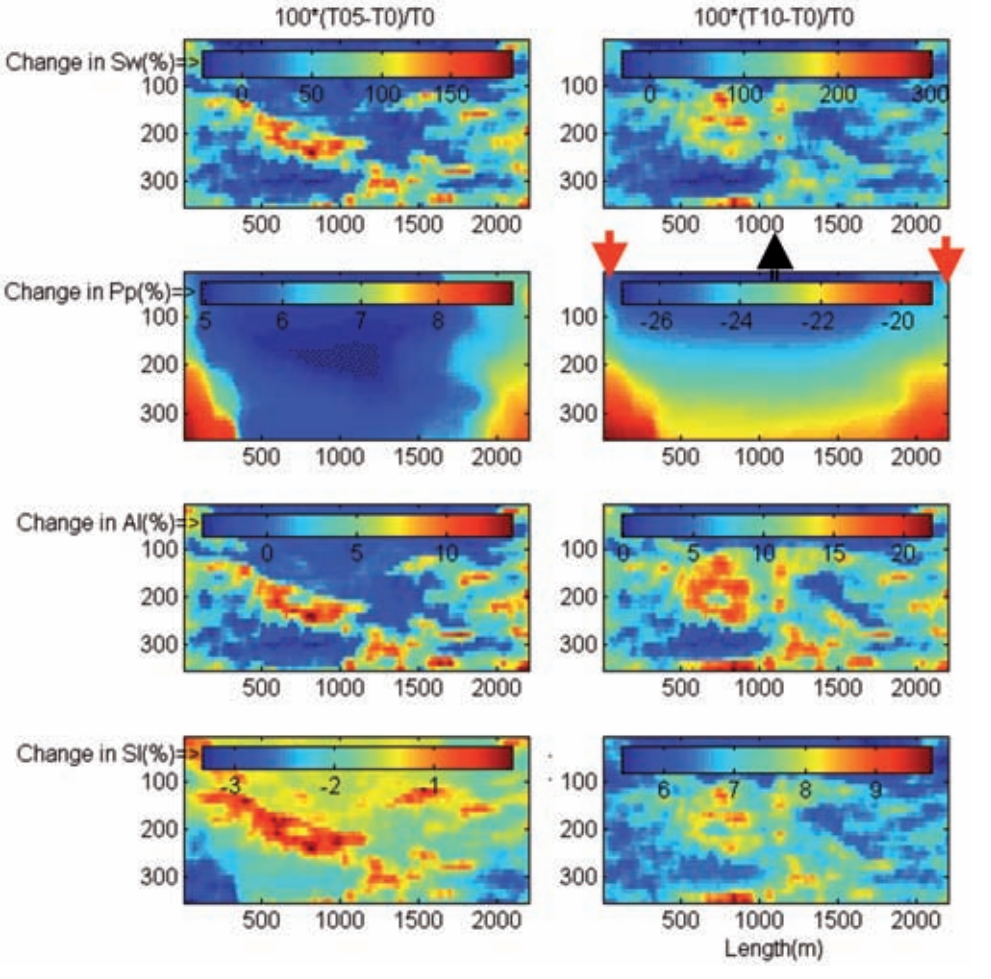

Fig. 1. Time-lapse normalized percentage changes in effective water saturation, Sw, (upper row), pore pressure, Pp, (2nd row from top), and the associated changes in seismic acoustic impedance, AI, (3rd row from top) and shear impedance, SI, (lower row) between base survey and monitor survey after 5 years of waterflooding (left column) and between base survey and monitor survey after 10 years (right column). X- and Y-axes are the same for all panels and they are reservoir length and thickness in meters, respectively. Each panel is color-coded for the corresponding attribute. Red and black arrows indicate the locations of the injector and producers wells, respectively.

SEISMIC MODELING

Here we explore the use of 1D and 2D seismic modeling and their effects on the time-lapse signatures associated with waterflooding into a black oil reservoir. To do so, the developed petro-elastic model are embedded into a 1D background elastic model simulating surrounding offshore sedimentary basin in which the reservoir is buried (Fig. 2). The background model has dimensions of 600 × 300 in length and depth respectively. The grid size is the same as the reservoir model 10 × 10 m². The first one kilometer of the model is sea water. The reservoir is located at a depth of 2000 m of the background model and sandwiched between an ash and salt layers at top and bottom, respectively. These two markers help to track the reservoir on various seismic responses. The edges of the reservoir are smoothed by a linear interpolation scheme to better blend with the background model.

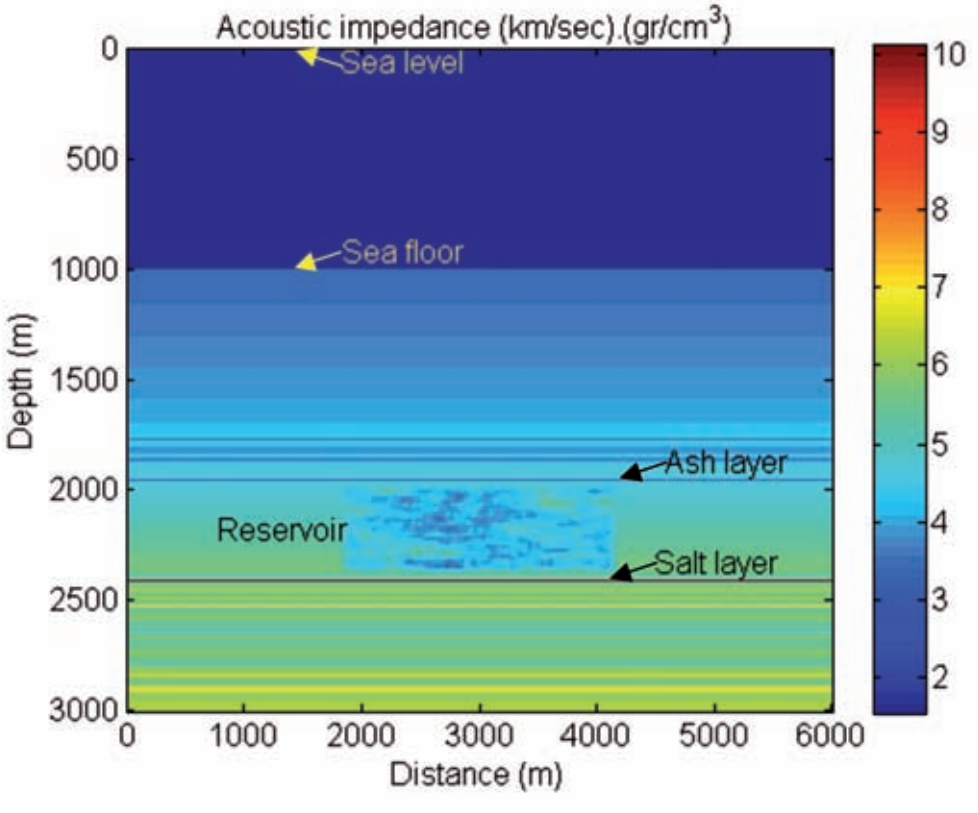

Fig. 2. Petro-elastic model embedded into a 1D background elastic model simulating surrounding offshore sedimentary basin. The background model has dimensions of 600×1×300 in length, width, and depth, respectively. The grid size is the same as reservoir model 10×10×10 m³. The first one kilometer of the model is sea water. Reservoir was embedded at depth 2000 m of the background model and sandwiched between an ash and salt layers at top and bottom, respectively. The edges of the reservoir were smoothed to better blend with the background model.

One-dimensional seismic modeling

The most widely used earth model in petroleum exploration is a horizontally-stratified model representing a typical sedimentary basin in which a reservoir is buried. The corresponding approach to computing the seismic response in such a media is called one-dimensional seismic forward modeling and is well studied in the open technical literature, e.g., Kennett (1985) and Chapman (2004).

In this paper, we utilize 1D modeling approach to simulate pre-stack seismic data in the intercept time and horizontal ray parameter domain, called $\tau-$p. The first modeling approach is to simulate acoustic wave propagation without internal multiples. Here, the frequency domain is used to construct a primaries-only wavefield, i.e., acoustic P-P reflection coefficients, for all depth levels in the 1D model. The intercept times are calculated by 1D ray tracing. After collecting the wavefield at all desired frequencies for each ray parameter being simulated, an inverse 1D Fourier transform over frequency is applied to obtain the wavefield in intercept time. The outermost loop in the algorithm is over horizontal ray parameter (p), allowing us to generate data for all the ray parameters of interest.

The second modeling approach is to simulate acoustic wave propagation with internal multiples. Similar to the above method, the primary wavefield is simulated and internal multiples are also simulated by including a recursive term for each layer into the frequency domain equations (Kennett, 1985).

The third algorithm simulates elastic wave propagation without internal multiples. Here, full Zoeppritz equations to compute elastic P-P reflection coefficients and 1D ray tracing to calculate intercept times, are employed.

The ultimate 1D modeling option is to generate the full elastic reflectivity response of the stratified media. The corresponding seismic response is theoretically exact for 1D media because the internal multiples and mode-converted events are modeled (see Kennett, 1985 and Chapman, 2004, for more detail).

To simulate the production-induced seismic response of the reservoir, we implement a locally 1D modeling over the 2D reservoir models associated with a base and two monitor surveys after 5 and 10 years of waterflooding. As mentioned earlier, our 1D modeling methods generate seismic data in the $\tau-$p domain. Fig. 3 displays plane-wave response of the 1D locally model in the middle of the 2D reservoir for the base survey (T0). The $\tau-$p response is simulated by full elastic reflectivity algorithm for a flat frequency range of 0 to 75 Hz. Markers on the seismic data show significant events associated with 2D model in Fig. 2. To evaluate the full range of pre-stack data, we select four ray

parameters of 0.0, 0.10, 0.20, and 0.30 s/km. These ray parameters are associated with different incident angles at sea level and at the reservoir top. Using 1D ray tracing equations, we also compute the corresponding intercept times, offsets, and traveltimes for the selected ray parameters and up to the reservoir top. Table 1 summarizes the geometry of data to be selected for further analysis. For the rest of the analysis of 1D seismic responses of the reservoir, we will concentrate on a time window from reservoir top to bottom.

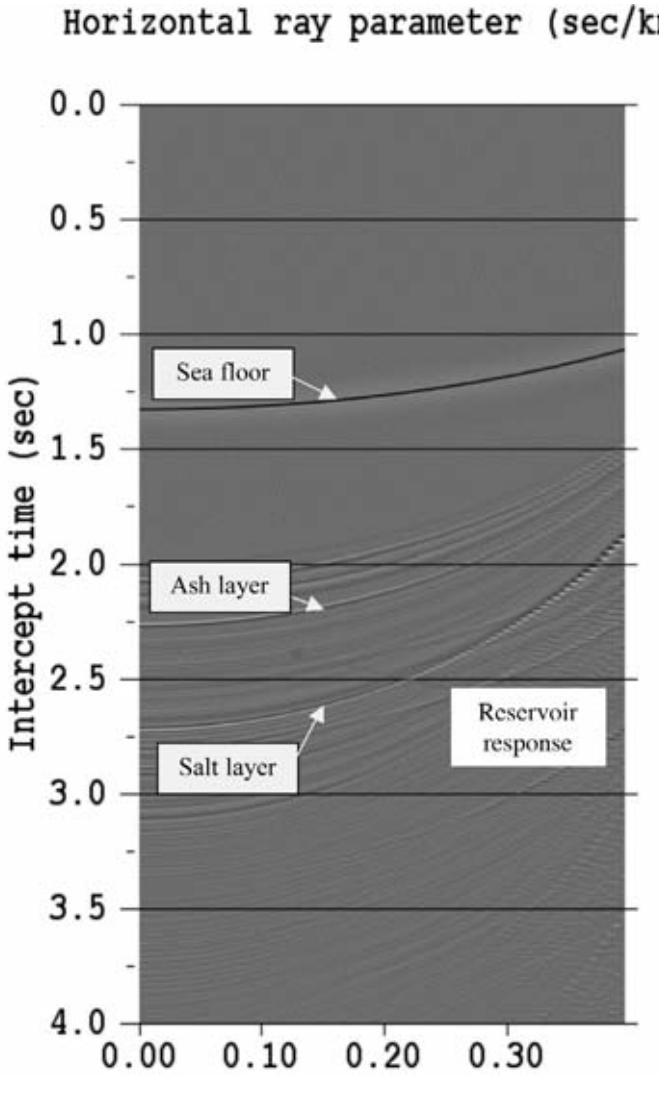

Fig. 3. Plane-wave response of the 1D locally model in the middle of 2D reservoir for base survey (T0). The response was simulated by full elastic reflectivity algorithm for flat frequency of 0 to 75 Hz. Markers on the seismic data shows significant events associated with 2D model in Fig. 2. No gain is applied to the data. For display purpose a band-pass filter of 5 to 65 Hz is applied.

Table 1. Geometry of different pre-stack traces simulated by 1D and 2D plane-wave seismic modeling techniques.

	First trace	Second trace	Third trace	Fourth trace
Ray parameter (s/km)	0.0	0.10	0.20	0.30
Offset (km)	0.0	0.721	1.526	2.565
Incident angle at sea level (degrees)	0.0	8.7	17.4	26.7
Incident angle at reservoir top (degrees)	0.0	11.8	24.1	37.8
Intercept time (sec)	2.314	2.278	2.167	1.965
Traveltime (sec)	2.314	2.350	2.472	2.735

This window has a fixed interval, but its starting level is ray parameter-dependent. This scheme allows one to analyze the raw seismic data without any seismic data processing, e.g., normal moveout correction; consequently, the time-lapse signatures will be preserved. This is important to compare time-lapse signature using various plane-wave seismic modeling in the $\tau-p$ domain and also consistent with our further analysis in offset-traveltime domain for finite difference data to be discussed later. The 1D plane-wave seismic modeling is carried out for a flat frequency range of 0 to 75 Hz and recorded at all 600 horizontal grid positions (every 10 m) at sea level. Finally, a normalized derivative of a Gaussian wavelet with a peak frequency of 35 Hz is convolved with data (Fig. 4). The same wavelet will be convolved with 2D plane-wave and used, as a source, to simulate 2D finite difference data to be discussed later.

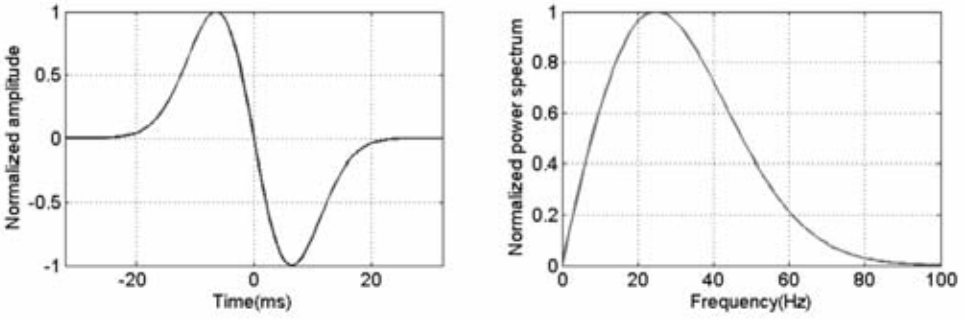

Fig. 4. Normalized derivative of a Gaussian wavelet with a peak frequency of 35 Hz convolved with 1D and 2D plane-wave seismic data and used, as a source, to simulate 2D finite difference data.

Due to the fact that our 1D modeling algorithms are generated using different numerical methods, we expect to have slightly different amplitude scales. To overcome this problem we use the sea floor amplitude as a tuning parameter and scaled data accordingly. Form the physics of the seismic modeling, we expect to have the same response from 1D acoustic without multiples (called method 1DAp; A stands for Acoustic and p stands for primary) and 1D elastic without multiples (called method 1DEp; E stands for Elastic) at zero ray parameter. In addition 1D full elastic reflectivity algorithm (called method 1DEpmc; m, and c stand for internal multiples and converted waves, respectively) should converge to 1D acoustic with multiples (called method 1DApm) at $p = 0$, because no converted wave is generated. Fig. 5 illustrates the scaling scheme employed in this study for a single trace in the middle of the 2D reservoir. Method 1DEpmc perfectly coincides on 1DAm for the entire survey (not shown here). However, this is not the case between 1DAp and 1DEp (the second panel in Fig. 7). This is explained by the fact that we use a time-domain modeling, 1D ray tracing algorithm to compute 1DEp and a frequency domain method for 1DAp. In other words, numerical differences between these two algorithms lead to a minor difference between these two surveys, but this will not affect our analyses as long as we are aware of its existence.

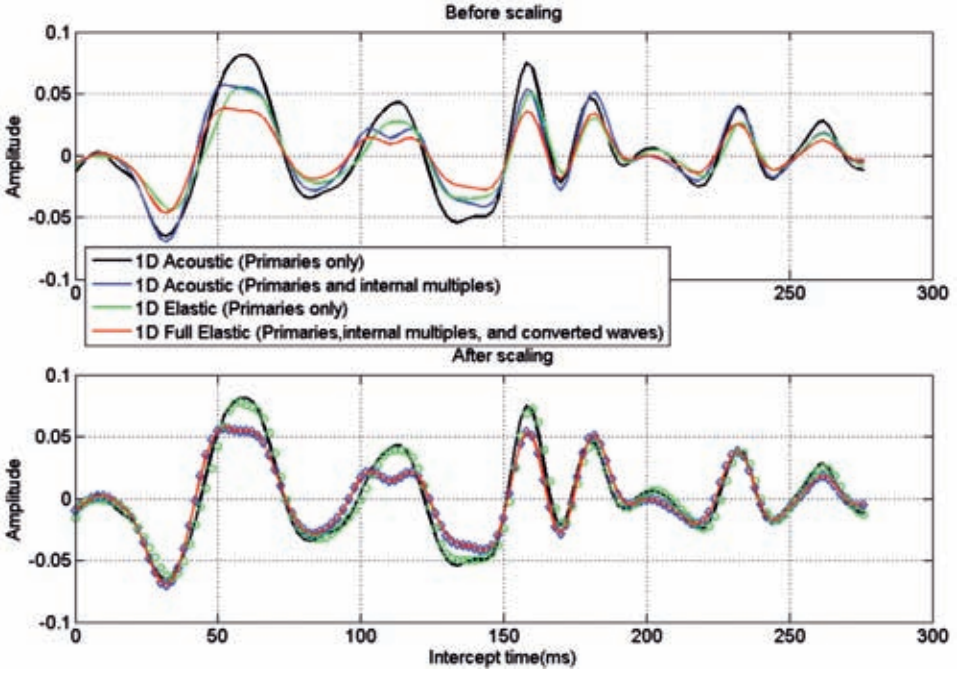

Fig. 5. The scaling scheme used to tune 1D plane-wave seismic data computed from various algorithms.

Fig. 6 shows the plane-wave responses of different modeling methods computed for base survey (T0) at p = 0 s/km. We only display the reservoir zone in both temporal and lateral axes. The reservoir response looks very realistic with all the complicated structures inherent in actual petroleum reservoirs. This is mainly because of spatial distributions of and correlations between reservoir properties used in the developed petro-elastic model. Comparing 1DAp and 1DEp, and by introducing the internal multiples in 1DApm and 1DEpmc tends to attenuate primary amplitudes. As mentioned above, 1DEpmc data is scaled to 1DAm, so these two data sets are exactly the same for the entire base and monitor surveys at p = 0. The same statement is true for 1DEp and 1DAp. However, there are minor numerical differences between these two data sets as explained above.

To highlight the effects of internal multiples, acoustic versus elastic wave propagation, and converted waves, we will display the residual sections associate with different seismic modeling techniques. Fig. 7 shows the residual

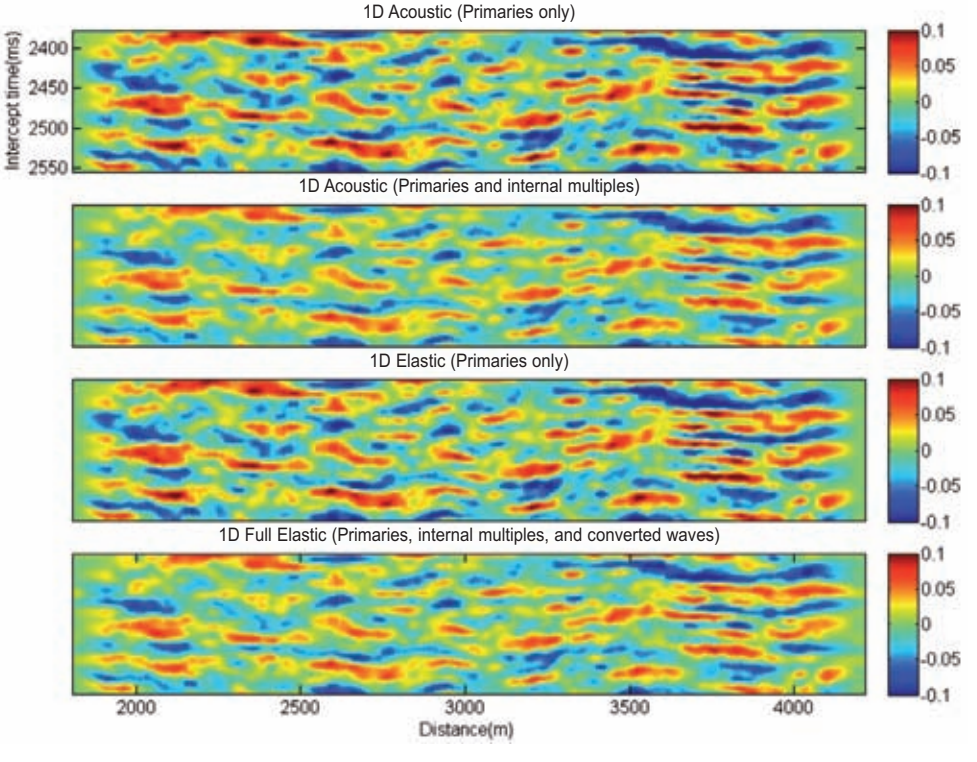

Fig. 6. 1D plane-wave responses of the base survey (T0) at ray parameter (p = 0 s/km) computed by different seismic modeling methods.

between the plane-wave responses shown in Fig. 6 for base survey (T0) at p= 0 s/km. The first panel is the residual between 1DAp and 1DApm, and one can clearly see the internal multiples created in reservoir zone. Some of the coherent and linear ones may be generated due to contrast at reservoir top or even ash layer above the reservoir (see Fig. 2). The minor ones may be generated due to the local big contrasts within the reservoir. The second panel displays the residual between 1DEp and 1DAp, and as expected this is almost zero everywhere because no difference exists between elastic and acoustic wave propagation at p = 0. The third panel illustrates the residual between 1DEp and 1DEpmc. Similar to panel one, internal multiples are the residual, but this time they are computed by full elastic reflectivity algorithm. Similarities between panels 1 and 3 confirm that our modeling algorithms are consistent. The last panel in this figure indicates the effect of converted waves. This panel is computed from the residual of the first and third panel. The common terms in these two panels, primary and internal multiples subtract out, so the remainder

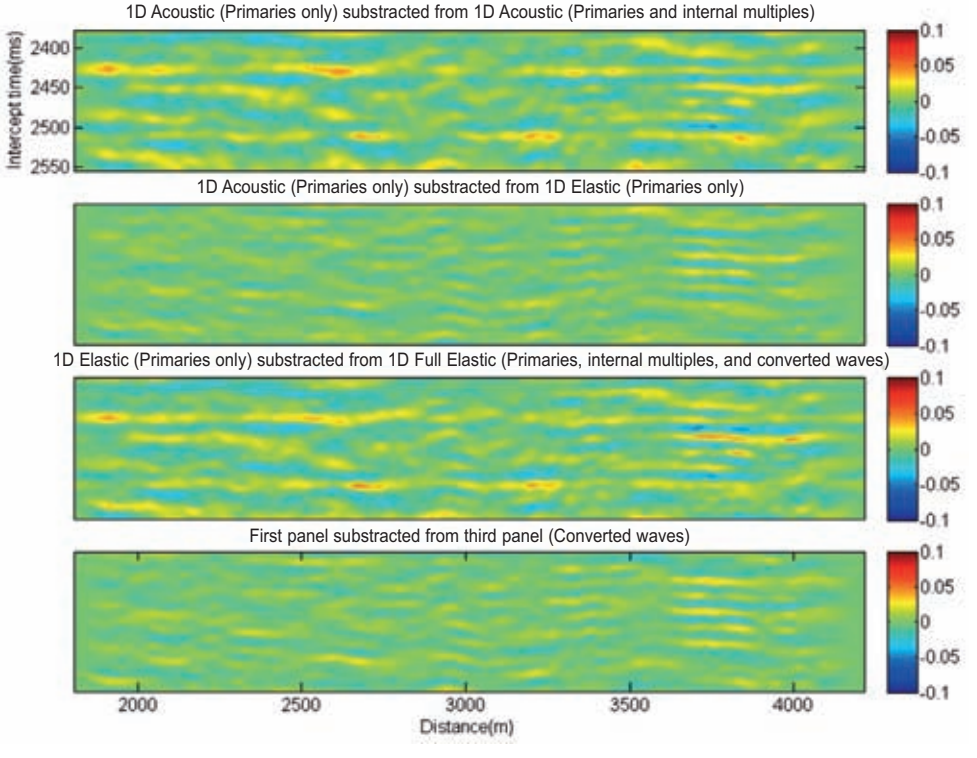

Fig. 7. Residuals of 1D plane-wave responses of the base survey (T0) at ray parameter (p = 0 s/km) computed by different seismic modeling methods.

can be a first order approximation of the converted waves, if any. We emphasize that this is only an approximation because internal multiples computed from 1DApm and 1DEpmc are not necessarily the same due to the fact that internal multiples of converted waves are not modeled by 1DApm. There is no converted wave at p = 0, so the last panel must be zero everywhere. This isn't the case here as mentioned earlier due to numerical error propagated from differences between two algorithms of 1DAp and 1DEp. Consequently, panels 2 and 4 are similar.

Figs. 8 to 10 show the same kind of residual sections, as Fig. 7, between plane-wave responses for base survey (T0) and for p = 0.1, 0.2, and 0.3 s/km, respectively. The goal here is to investigate the effect of internal multiples, elastic vs. acoustic wave propagation, and converted waves at larger ray parameters. The same events on the p = 0 section appear at earlier intercept times at larger ray parameter. This is because of elliptical trajectories in the $\tau - p$ domain. In general, internal multiples, converted waves, and elastic effects

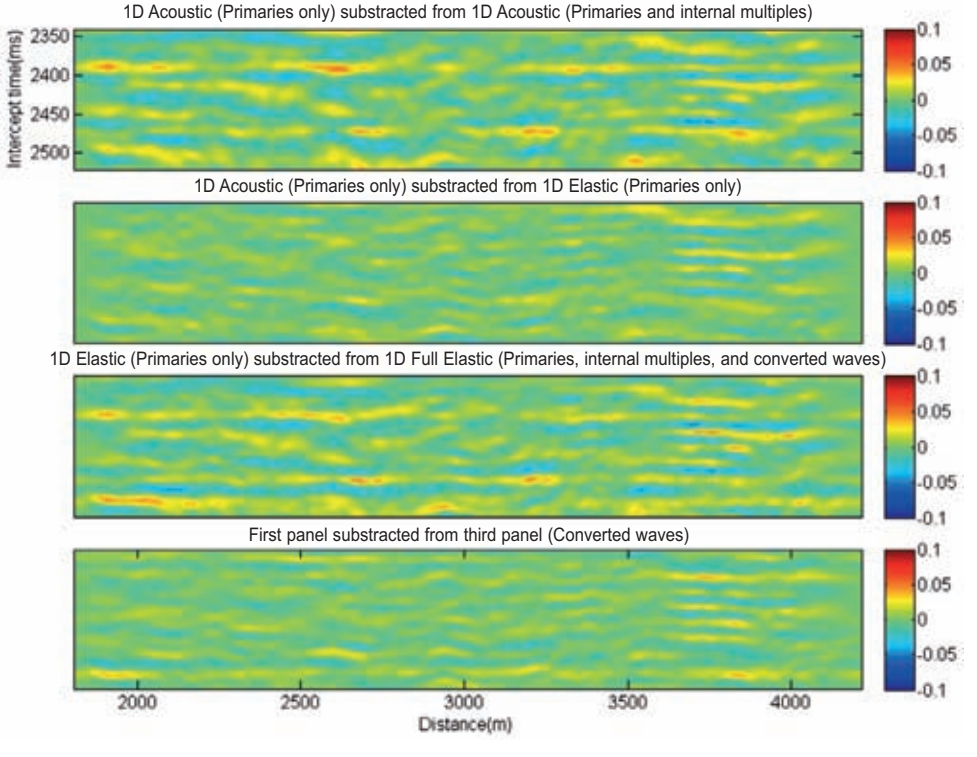

Fig. 8. Residuals of 1D plane-wave responses of the base survey (T0) at ray parameter (p = 0.1 s/km) computed by different seismic modeling methods.

are more observable at larger ray parameters, however; this is not a linear relationship. At p = 0.1 s/km, elastic and acoustic wave propagation types are approximately similar to p = 0. Converted waves are not generated. At p = 0.2 s/km, we start seeing some noticeable differences between elastic and acoustic wave propagation. This effect is more significant than internal multiples in some parts of the reservoir, e.g., coherent peak event at upper right indicated in red. At p = 0.3 s/km, differences between elastic and acoustic wave propagation is the most dominant effect. Here, converted waves are generated with significant amplitudes compared to primaries and internal multiples. At p = 0.2 and 0.3 s/km, there are coherent horizontal events in the last panel. They are expected to be converted waves, but they are residual of internal multiples modeled by 1DEpmc but not modeled by 1DApm algorithm.

The above observations based on the simulating different seismic modeling for the base survey (T0), confirms that modeling of internal multiples

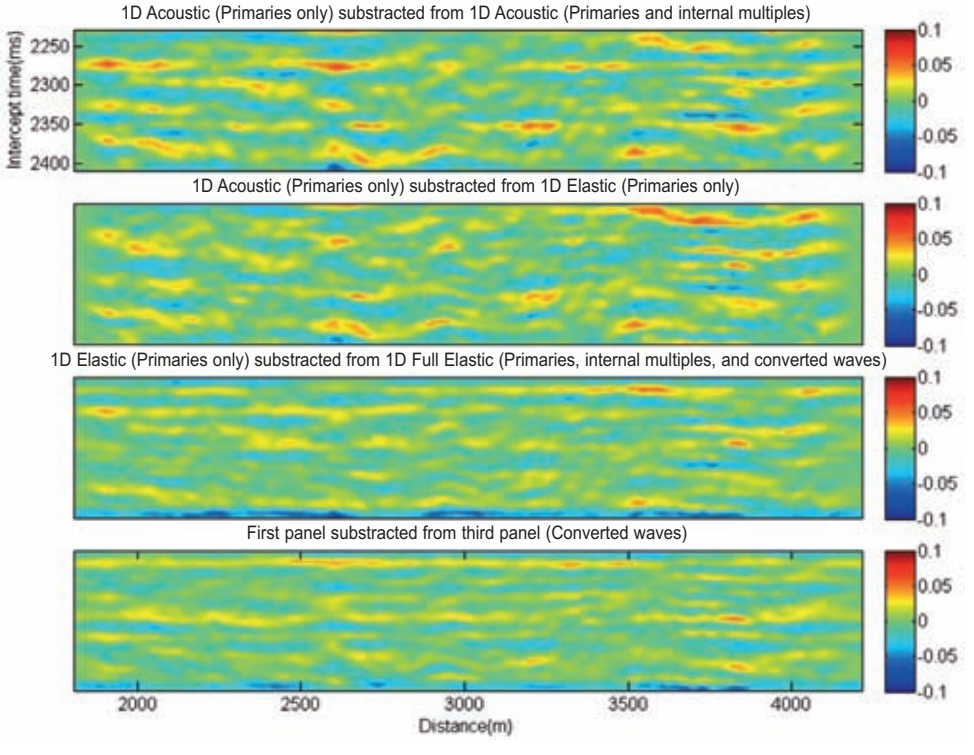

Fig. 9. Residuals of 1D plane-wave responses of the base survey (T0) at ray parameter (p = 0.2 s/km) computed by different seismic modeling methods.

matters in seismic reservoir characterization projects. They are small at p = 0 s/km but nonetheless observable. The larger the ray parameter, the higher the amplitude of the internal multiples. The acoustic wave propagation is a good approximation to model a 1D elastic medium up to p = 0.1 s/km. However, this assumption is not valid beyond p = 0.1 s/km. Finally, converted waves are rarely produced between p = 0.1 and p = 0.2 s/km, so a primary plus multiples analysis only should be enough in this ray parameter range. Converted waves are significant beyond p = 0.2 s/km and their ignorance may seriously impact our analyses.

The key question for this study is whether or not the same statements are true in reservoir monitoring projects. In other words, can we show that internal multiples and converted waves are less important in time-lapse seismic modeling because they subtract out between the base and monitor survey, so a primary wavefield analysis should be enough. To investigate this hypothesis, we repeat the experiment for one set of time-lapse.

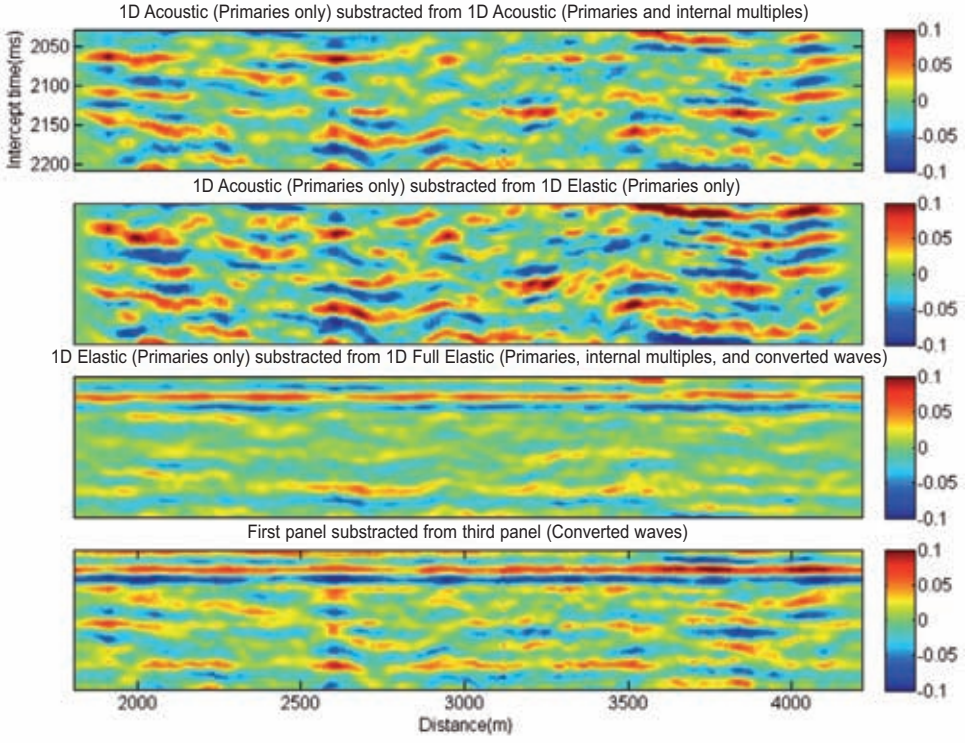

Fig. 10. Residuals of 1D plane-wave responses of the base survey (T0) at ray parameter (p = 0.3 s/km) computed by different seismic modeling methods.

Fig. 11 shows the plane-wave responses of different modeling methods computed for time-lapse (T5-T0), associated with the base and the monitor survey after five years of waterflooding, at p = 0 s/km. By comparing to Fig.1, one can easily track waterfront location and distinguish between the unflooded areas and flooded zones at the back of waterfront. As expected, 1DAp and 1DEp are the same because there is no difference between acoustic and elastic wave propagation at p = 0.0 s/km. Also, 1DEpmc and 1DApm are similar because of the lack of converted waves at zero ray parameter.

Figs. 12 to 15 show the residuals between time-lapse surveys computed by different seismic modeling algorithms for p = 0.0, 0.1, 0.2, and 0.3 s/km, respectively. In other words, a set of base and monitor surveys are first computed by, say, algorithm A, and then computed by algorithm B. If we subtract these two time-lapse surveys we should be able to track differences in fluid flow detection as simulated by seismic modeling algorithms A and B.

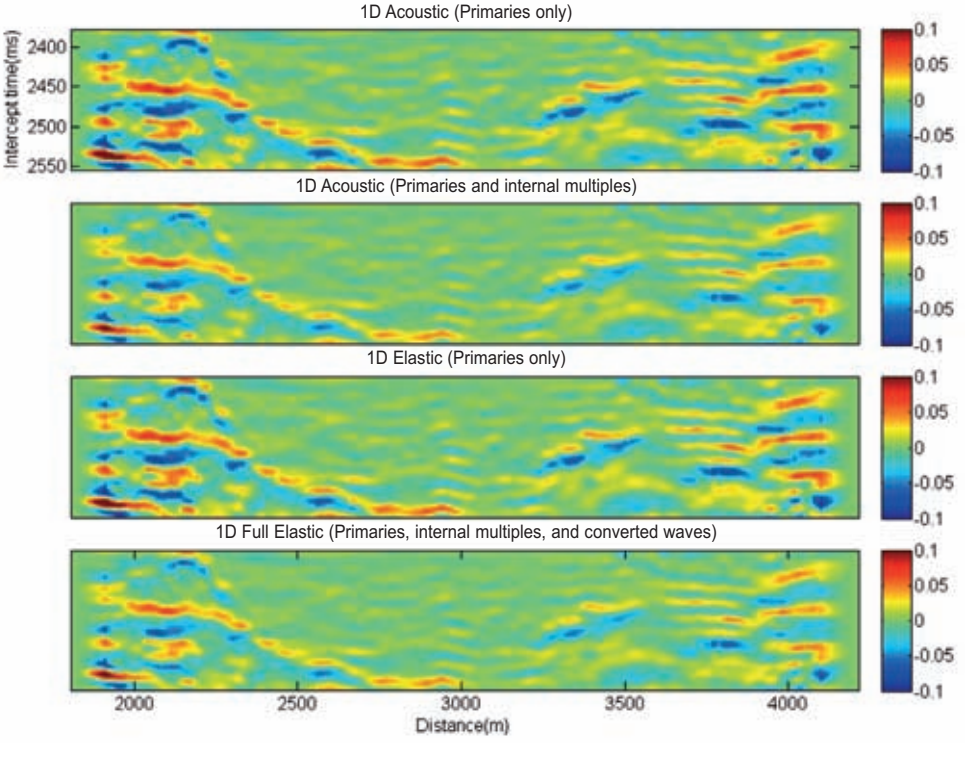

Fig. 11. 1D plane-wave responses of the time-lapse (T5-T0), base survey is subtracted from monitor survey after 5 years of waterflooding, at ray parameter (p = 0 s/km) computed by different seismic modeling methods.

Similar to the base survey in Figs. 8 to 10, internal multiples, converted waves, and elastic effects are more observable at larger ray parameters. At p = 0.0 s/km, internal multiples in unflooded zones areas completely cancel out each other. Internal multiples in the back of waterfront, flooded zones, partially subtract out and they are less significant than those of the base survey in Fig. 7. As discussed earlier, the second and third panels are supposed to be zero, but they are not due to numerical differences between algorithms 1DEp and 1DAp. At p = 0.1 s/km, elastic and acoustic wave propagation types are approximately similar to p = 0. Converted waves are not generated. At p = 0.2 s/km, we start seeing some noticeable differences between elastic and acoustic wave propagation. However, these differences are not as significant as the base survey in Fig. 9. That is, for time-lapse, acoustic modeling of an elastic medium is good approximation up to p = 0.2 s/km. At p = 0.3 s/km, differences between elastic and acoustic wave propagation once again becomes the most dominant effect. Here, converted waves are generated with significant amplitudes compared to primaries and internal multiples.

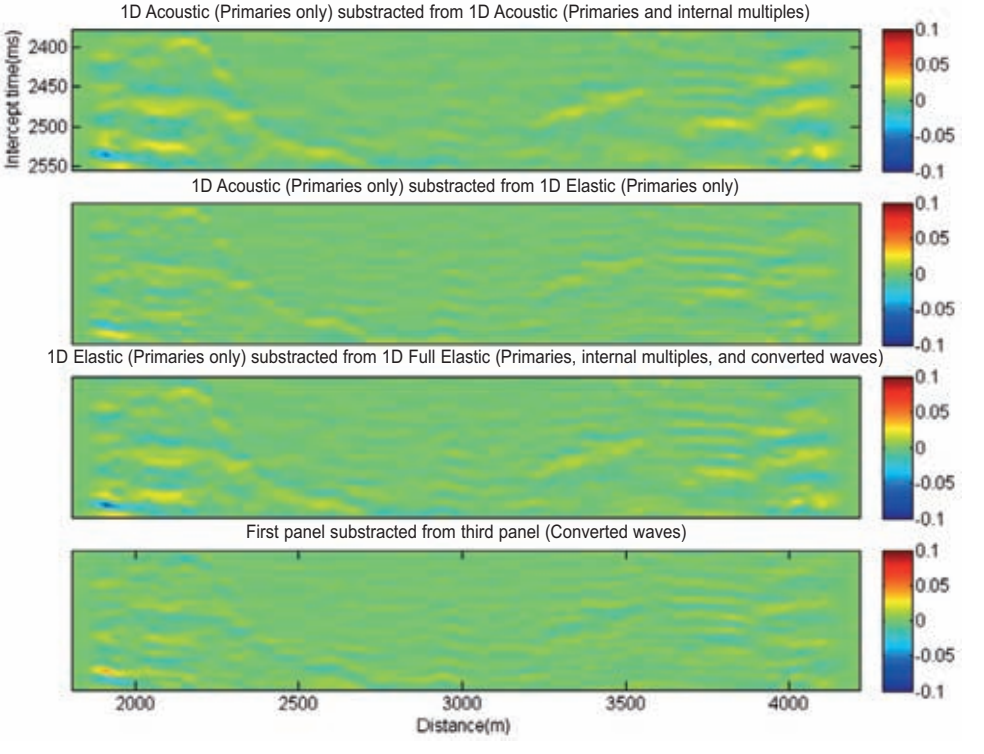

Fig. 12. The residuals of 1D plane-wave responses of the time-lapse (T5-T0), base survey is subtracted from monitor survey after 5 years of waterflooding, at ray parameter (p = 0 s/km) computed by different seismic modeling methods.

We emphasize that all internal multiples, elastic vs. acoustic modeling and converted waves show time-lapse signatures at the back of the waterfront. These time-lapse signatures are less noticeable at p = 0.0 and 0.1 s/km, but they are significant beyond p = 0.2 s/km.

2D seismic modeling

One-dimensional seismic modeling is an accurate approach for modeling layered sedimentary basins. Many sedimentary basins, however, are so structurally complicated that they can not be modeled by 1D modeling algorithms. In addition to the complexity of overburden of the petroleum reservoirs, the fluid flow phenomena itself has a 3D nature, so seismic time-lapse modeling has to be carried out using 3D or at least 2D modeling algorithms and compared against 1D responses. By doing so, we can highlight the differences in modeling for time-lapse purposes. To address this problem,

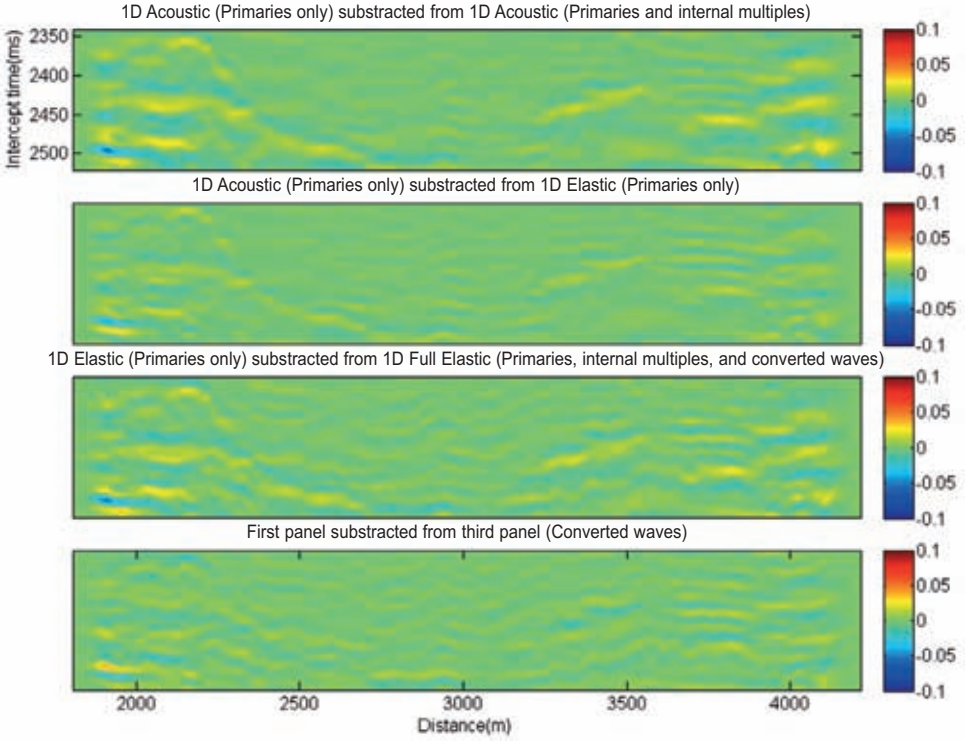

Fig. 13. The residuals of 1D plane-wave responses of the time-lapse (T5-T0), base survey is subtracted from monitor survey after 5 years of waterflooding, at ray parameter (p = 0.1 s/km) computed by different seismic modeling methods.

many forward modeling approaches, ray theory, integral equations, finite difference, finite element, etc., can be utilized to evaluate numerical approximations of wave equations (see Carcione et al. (2002) for an overview on seismic modeling methods).

In this paper, we utilize two seismic modeling techniques, a semi-analytical method based on plane-waves originally used in split-step Fourier migration (Stoffa et al., 1990) and a purely numerical approach, staggered grid explicit FD (Levander, 1988).

Stoffa et al. (1990) developed split-step Fourier migration to migrate zero-offset seismic data. The method is an extension of Gazdag's phase shift migration to handle lateral velocity variations. In their method, a 3D slowness model is first decomposed to a 1D, depth-dependent, mean slowness and a perturbation term representing the local variability of slowness. Downward continuation of the wavefield across each depth interval by performing a global

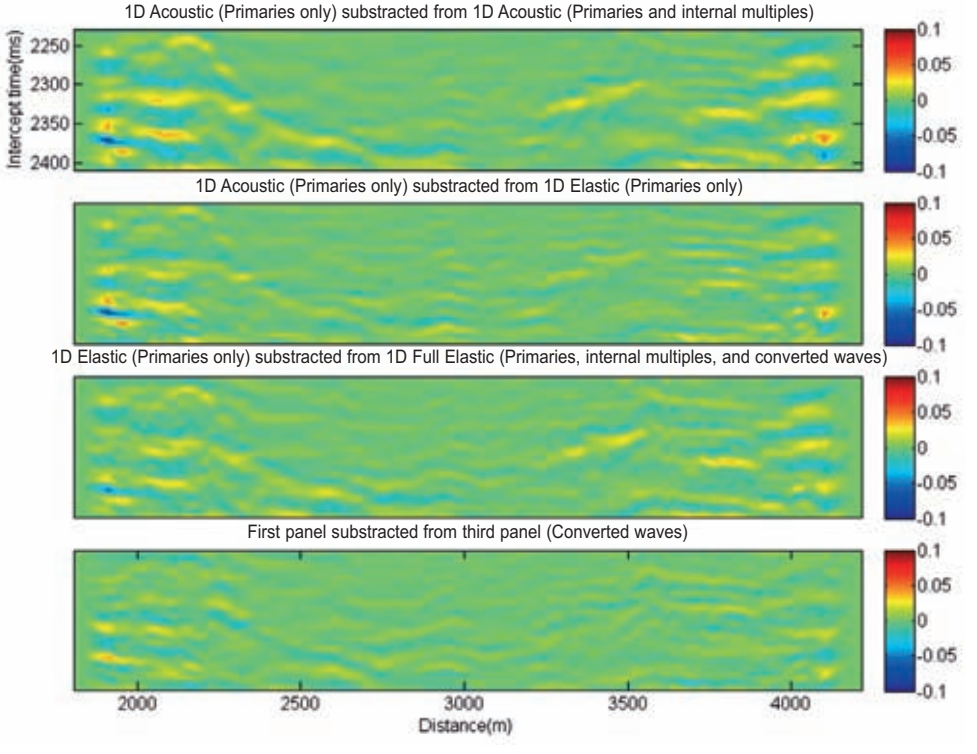

Fig. 14. The residuals of 1D plane-wave responses of the time-lapse (T5-T0), base survey is subtracted from monitor survey after 5 years of waterflooding, at ray parameter (p = 0.2 s/km) computed by different seismic modeling methods.

phase shift using the mean slowness in the frequency-wavenumber domain is followed by a local phase shift based on the slowness perturbation component in the frequency-space domain. The extension of this method to accommodate pre-stack seismic imaging is reported in open technical literature, e.g., Tanis et al. (1998), etc. However, the use of this algorithm as a seismic forward modeling has not yet been published. Here in this paper, we first explain the algorithm and then apply it on several 2D geological models associated with a base and two monitor surveys.

The Split-step Fourier plane-wave (SFPW) seismic modeling algorithm is described schematically in Fig. 16. Initially full elastic reflection coefficients are computed for the geological model. For each depth interval and in space-frequency domain wavefield is updated by applying a local phase shift accounting for local variability of the slowness component. Next, the wavefield is transformed into wavenumber domain where a global phase shift associated

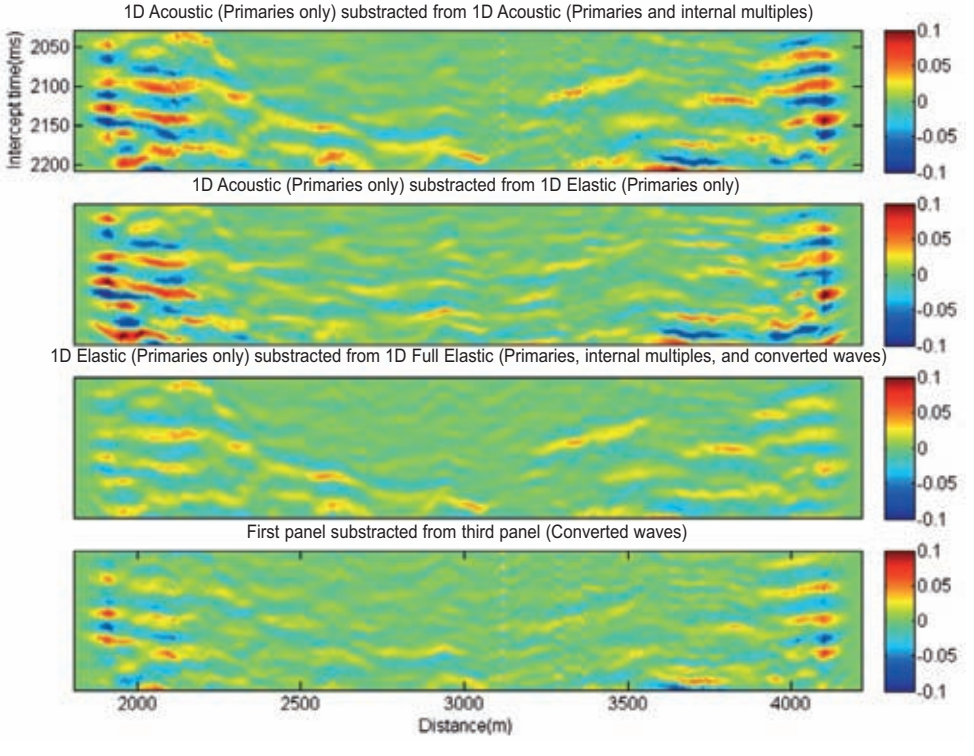

Fig. 15. The residuals of 1D plane-wave responses of the time-lapse (T5-T0), base survey is subtracted from monitor survey after 5 years of waterflooding, at ray parameter (p = 0.3 s/km) computed by different seismic modeling methods.

Split-step Fourier plane-wave (SFPW) seismic modeling algorithm

Compute elastic reflection coefficients using full Zoeppritz equation for the cube of geological model at all X (x, y) positions, over depth z, and for all ray parameters (p), $\mathrm{RC}(\mathrm{X}, z, \mathrm{p})$

Initialize the pressure wavefield, for all frequencies (ω) and all ray parameters (p), $P(X,\omega,p) = complex(0.,0.)$

- Loop over ray parameter
  - Loop over frequency
    - Loop over depth (from bottom to top)
      - Loop over X

        Apply local phase shift in frequency-space domain

        $P(X,\omega,p) = P(X,\omega,p) + RC(X,z,p)\times\exp(-i\omega\Delta u(X,z)\Delta z)$

        Add internal multiples if needed
      - End loop over X

      Space (X) to wavenumber (K_X) FFT
      - Loop over K_X

        Apply global phase shift in frequency-wavenumber

        $P(K_X,\omega,p) = P(K_X,\omega,p)\times\exp(-i\omega\Delta z\sqrt{\omega^2 u_{mean}^2 - K_X^2})$
      - End loop over K_X

      Wavenumber (K_X) to Space (X) FFT
    - End loop over depth
  - End loop over frequency
  - Loop over X

    Add surface multiples if needed

    Frequency to intercept time (τ) FFT

    Collect wavefield $P(X,\tau,p)$
  - End loop over X
- End loop over ray parameter

Fig. 16. A pseudo FORTRAN code for Split-step Fourier plane-wave (SFPW) seismic modeling.

with mean slowness of the depth interval is performed in frequency-wavenumber. The wavefield is then back-transformed into space-frequency domain. After collecting all frequencies, the wavefield is transformed to intercept time. The entire process can be repeated to obtain the wavefield at different ray parameters allowing one to simulate pre-stack seismic data in the $\tau-$p domain.

The salient features of SFPW are as follows:

* Full elastic P-P reflection coefficients are utilized in acoustic wave equation, leading to an accurate approximation of the wavefield in complex geological models with low to moderate lateral variations. Shear amplitude loss is accounted for by using the Zoeppritz equations to define the P-wave reflection coefficients.

* Computational time of SFPW is very low and it can simulate, in a reasonable time, seismic data over 2D and 3D geological models of interest in petroleum industry. Modeling can be performed over a few ray parameters and over any desired frequency range, giving more flexibility and speed. In addition, it is naturally parallelizable over ray parameters and over frequencies. Finally, it is possible to move down to the target in one or several large steps using the average slowness of the corresponding depth interval. In marine seismic modeling, it is possible for example to model the water column in one large step.

* Internal and surface multiples can be either included or excluded from the computations.

* Diffractions are an internal part of the modeling, making SFPW a superior algorithm to locally 1D seismic modeling methods.

* Having superior speed to FD, and the ability to model higher frequencies than FD, SFPW is a good a candidate for seismic reservoir characterization and monitoring workflow.

We carry out 2D plane-wave seismic modeling using in-house SFPW code, called PW3D. To be consistent with 1D plane-wave modeling discussed earlier, a flat frequency range of 0 to 75 Hz is simulated and data were recorded at all 600 horizontal grid positions (every 10 m) at sea level at the top of 2D geological models associated with a base and two monitor surveys after 5 and 10 years of waterflooding. Finally, a normalized derivative of a Gaussian wavelet with a peak frequency of 35 Hz is convolved with the data (Fig. 4). Similar to 1D analyses, four ray parameters of 0.0, 0.10, 0.20, and 0.30 s/km are selected. These ray parameters are associated with different incident angles, intercept times, offsets, and consequently traveltimes for the reservoir top (Table 1).

Fig. 17 shows the plane-wave responses for base survey (T0) and time-lapse (T10-T0), associated with the base and the monitor survey after ten years of water flooding, at p= 0 s/km. The first and the third panel are associated with 1DEp modeling and the second and forth panels are computed by SFPW algorithm, called 2DEp. In this algorithm we can optionally include or exclude internal multiples. Here, to be consistent with 1DEp, we exclude internal multiples. 2DEp data is scaled to 1DEp by tuning the sea floor amplitude. The most obvious difference between 1D and 2D elastic modeling are the diffractions; they can be generated at reservoir edges and also at scatter points inside the reservoir. The diffractions contaminate the region outside the reservoir as well as inside; this is why the inside is so different from 1DEp. One may argue that migration of the 2DEp data results in 1DEp data. That may be the case, but it is out of scope of this study. Diffractions for the time-lapse partially subtract out, but not completely. This is because of the fact that diffractions for the base survey (T0) and monitor survey (T10) have some common parts, but they are a bit different as reservoir properties are different.

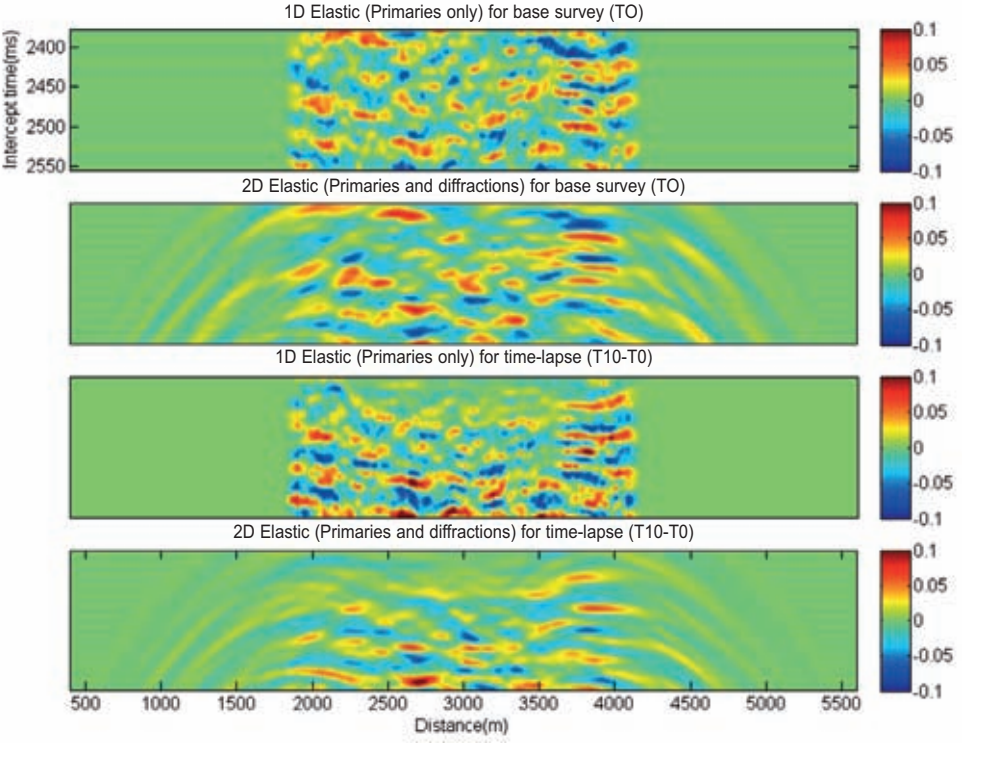

Fig. 17. Plane-wave responses for base survey (T0) and time-lapse (T10-T0), associated with the base and the monitor survey after ten years of water flooding, at p = 0 s/km. The first and the third panel are associated with 1D modeling and the second and forth panels are 2D modeling computed by SFPW algorithm.

Fig. 18 and Fig. 19 show 2DEp (primaries) and 2DEpm (primaries and internal multiples) at p = 0 s/km for base survey (T0) and time-lapse (T10-T0), respectively. One can easily see that internal multiples not only cancel out each other in the unflooded zones, but also they subtract out in flooded zones, so they are not a problem in the time-lapse analysis for small ray parameters. However, as demonstrated in 1D analyses, the internal multiples will be more pronounced at larger ray parameters.

The final seismic modeling technique employed in this study is a purely numerical approach, staggered grid explicit finite difference, FD, (Levander, 1988). For this part, we utilize in-house code called FDPSV. A 2nd-order operator in time and 4th-order in space are used in a staggered grid scheme. The program will generate elastic waves for multiple source activations and the data can be collected for each source activation at multiple receiving arrays each having multiple detectors. Vertical and horizontal velocity, tractions and pressure data can be recorded at each detector as required. This scheme makes it possible to acquire multi fold surface data and downhole data simultaneously and to simulate the shooting of a seismic line. Snapshots of the wavefield can also be generated to monitor the waves as they propagate through the medium.

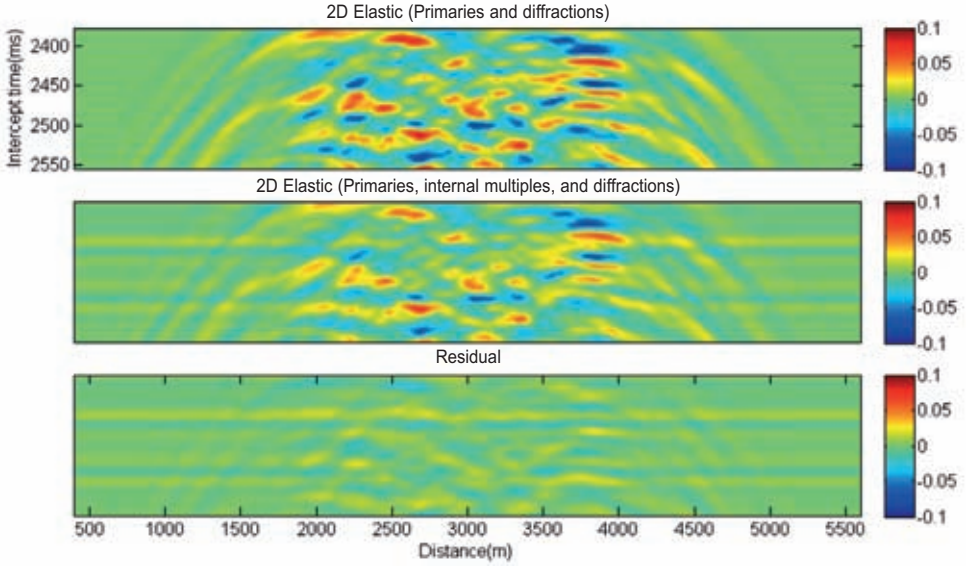

Fig. 18. 2D plane-wave responses, SFPW, for base survey (T0), at p = 0 s/km, without (first panel) and with (second panel) internal multiples. The third panel shows the residual of the first two panels, highlighting the internal multiples.

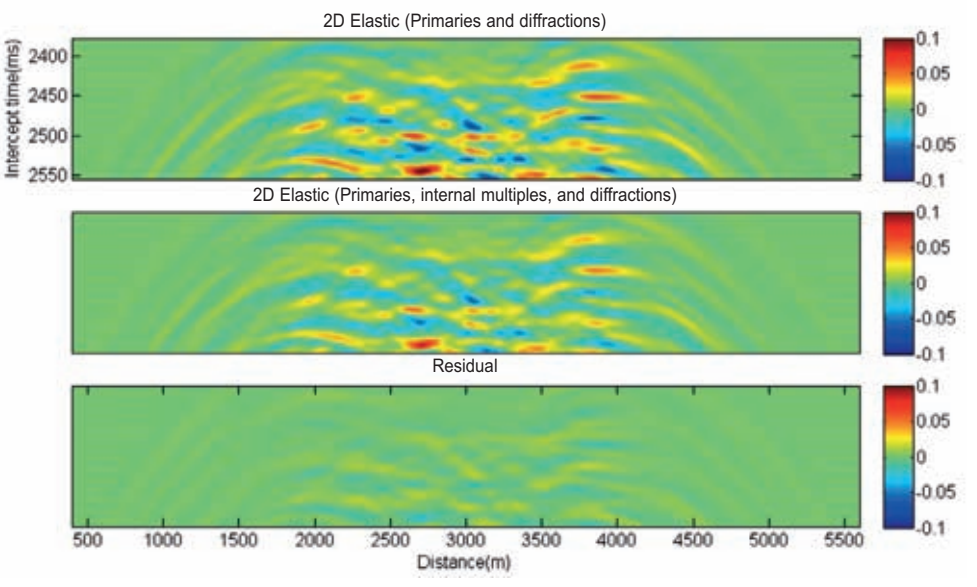

Fig. 19. 2D plane-wave responses, SFPW, for time-lapse (T10-T0), associated with the base and the monitor survey after ten years of water flooding, at p = 0 s/km, without (first panel) and with (second panel) internal multiples. The third panel shows the residual of the first two panels, highlighting the internal multiples.

The geological models associated with different production time steps, are tapered at the sides and the tops to attenuate artificial artifacts. In addition, models are extended at all sides to prevent backscattering waves from boundaries. For each geological model, 521 shots are acquired. Each shot position is evenly distributed at sea level located at the top of the models and spaced 10 meters apart, equal to grid size used in flow simulation. The pressure wavefield are recorded at 521 surface hydrophones at the sea level. All receivers were evenly distributed across the sea level and spaced 10 meters apart. To satisfy stability conditions given by $\alpha = C_{max}\Delta t/\Delta x \leq \sqrt{2}/\pi$, and considering $\Delta x = \Delta z = 10$ m, $C_{max} = 4600$ m/s for the salt layer beneath the reservoir, we employ $\alpha \leq 0.2$ (as recommended by Kosloff and Baysal, 1982), which results in $\Delta t \leq 0.4$ ms. Having computed the sample rate $\Delta t = 0.4$ ms, the maximum frequency to be recovered in seismic modeling without numerical dispersion, aliasing, is calculated using $f_{max} \leq C_{min}/2\Delta x$ and taking $C_{min} = 1500$ m/s, water velocity at the top of the model. The computed $f_{max} = 75$ Hz leads to choose the normalized derivative of a Gaussian wavelet with a peak frequency of 35 Hz, as a source (Fig. 4).

Fig. 20 illustrates finite difference response for a shot gather, located in the middle of 2D reservoir for base survey (T0). Pressure wavefield on shot gather is displayed. Markers on the seismic data shows significant events associated with 2D model in Fig. 2.

Fig. 21 compares the 2D plane-wave response computed by SFPW (2DEpm at p = 0.0 s/km) and finite difference responses (2DEpmc) of the base survey (T0) at zero offset, x = 0.0 km. These two data sets are inherently different because FD data has a cylindrical spreading divergence, but 2DEPm does not. In addition, our FD operator is an approximation of the derivatives of the wavefield in time and space. Finally, numerical dispersion and artifacts, common drawbacks of FD methods, are the other main difference between the FD and SFPW data. Consequently, one interested in making these two data sets

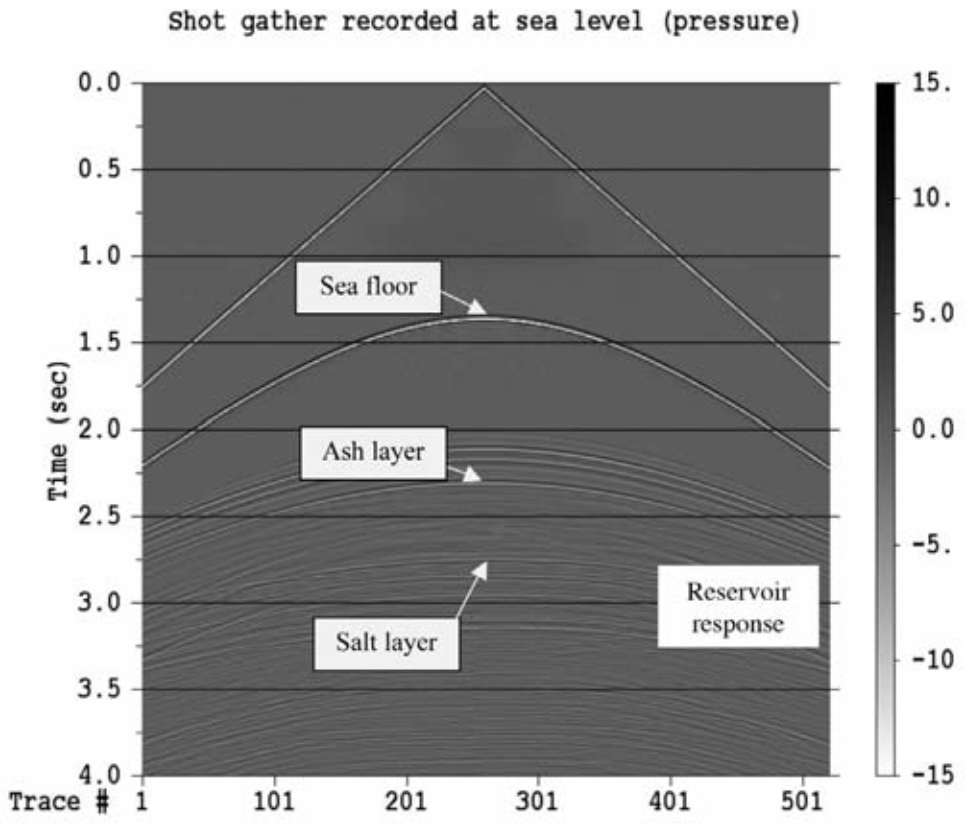

Fig. 20. Finite difference shot gather located in the middle of 2D reservoir for base survey (T0). Pressure wavefield is displayed. Markers on the seismic data shows significant events associated with 2D model in Fig. 2. For display purpose AGC of length 500 ms and band-pass filter of 5 to 65 Hz is applied.

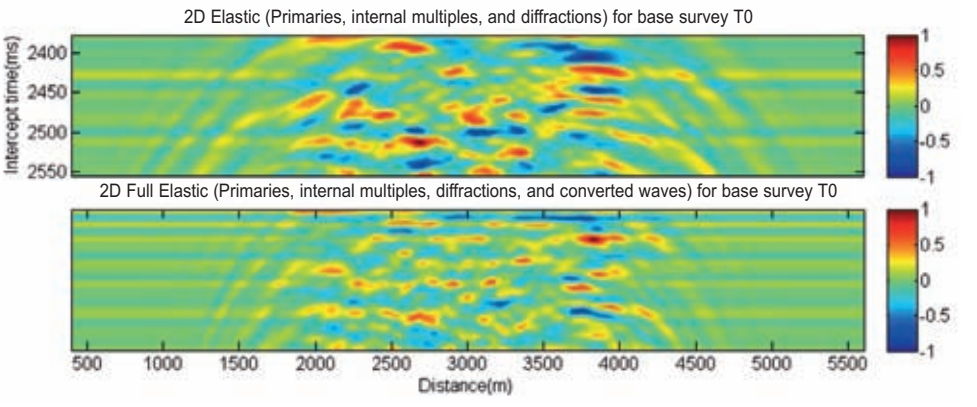

Fig. 21: 2D plane-wave, SFPW, (first panel) and finite difference (second panel) responses of the base survey (T0) at p = 0.0 s/km.

identical for quantitative comparison first needs to remove the 2D cylindrical spreading and correct FD to a true plane wave response by taking the appropriate plane wave transform of the FD data. In addition, we would need to use an FD operator accurate to the nyquist in space and time to get a response similar to the plane-wave algorithm. For an improved spatial response, one may consider pseudo-spectral Fourier (PSF) method (Chu and Stoffa, 2008) which helps to reduce numerical dispersion. These steps are out of scope of this study.

For our purposes we simply scale these two data sets by dividing each by its own maximum absolute value. This allows us to compare these data qualitatively. After scaling, most of the important features can be mapped between the two data sets. The main differences are in the arrival times and the dispersion in the FD data. The arrival times of the SFPW data is less accurate than FD because of the 1D with small later variation assumption. But, the dispersion in the FD split most of events and seems to be the most serious problem for matching the two data sets.

Fig. 22 compares the 2DEpm, SFPW, and 2DEpmc, FD, of the base survey (T0) at p = 0.0 s/km and for two monitor surveys associated with 5 and 10 years of waterflooding. As expected, due to subtraction the time-lapse response of SFPW and FD match better than the corresponding base surveys. This confirms that SFPW is able to model time-lapse responses of a complicated reservoir model and leads to comparable results as FD, but retains higher frequencies and is computationally much faster (a factor of 100 for our modeling).

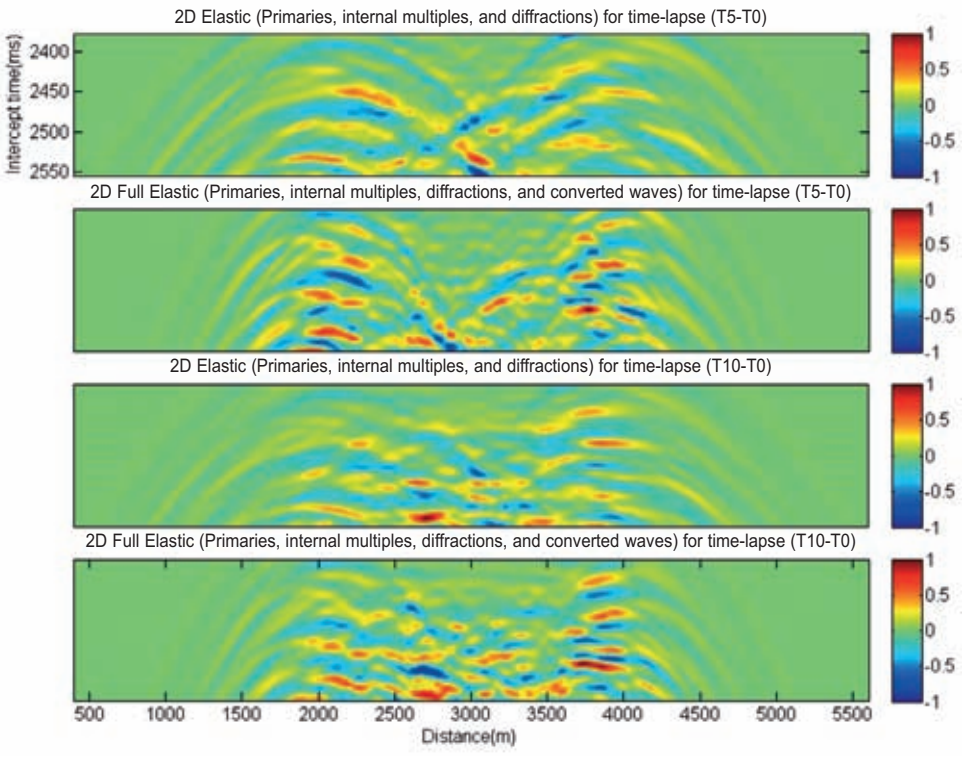

Fig. 22. 2D plane-wave, SFPW, (first and third panels after 5 and 10 years of waterflooding, respectively) and finite difference (second and forth panels after 5 and 10 years of waterflooding, respectively) seismic responses at p = 0.0 s/km.

SUMMARY AND CONCLUSIONS

The geologically consistent petro-elastic model employed here provide an opportunity to evaluate the effect of various seismic modeling techniques on a realistic reservoir model and investigate the corresponding time-lapse signatures due to waterflooding into a black oil reservoir.

Our analyses demonstrate that internal multiples in the back of waterfront, flooded zones, partially subtract out, so they are less significant in monitoring projects than reservoir characterizations.

We also find that for time-lapse seismic modeling, acoustic modeling of an elastic medium is a good approximation up to p = 0.2 s/km. In addition, at p = 0.3 s/km, differences between elastic and acoustic wave propagation is the most dominant effect. Here, converted waves are generated with significant amplitudes compared to primaries and internal multiples.

We also show that time-lapse modeling of the reservoir using SFPW approach is very fast compared to FD, 100 times faster for our case here, and it is capable of handling higher frequencies than FD. It provides an accurate image of the waterflooding process comparable to FD. Consequently, it is a powerful alternative for time-lapse seismic modeling.

As is the case for any seismic study, limitations include seismic noise, thickness tuning, and stiff rocks with low porosity. In addition, repeatability in seismic data acquisition and processing, and the low density contrast between hydrocarbon and injected fluid can limit the success of any seismic time-lapse project.

ACKNOWLEDGMENT

We would like to thank the sponsors of the UT-Austin EDGER Forum and the Jackson School of Geosciences at the University of Texas at Austin for their support of this research. Alireza Shahin sincerely thanks Carlos Verdin, Larry Lake, Jack Dvorkin, and William Galloway for enlightening discussion on reservoir modeling and rock physics. A note of special gratitude goes to Schlumberger for providing reservoir simulation software.

REFERENCES

Arps, J.J., 1953. The effect of temperature on the density and electrical resistivity of sodium chloride solutions. Petroleum Transactions AIME 198, 327-330.

Aziz, K. and Settari, A., 1979. Petroleum Reservoir Simulation. Applied Science Publishers Ltd., London.

Avseth, P., Mukerji, T. and Mavko, G., 2005. Quantitative Seismic Interpretation. Cambridge Univ. Press, Cambridge.

Batzle, M. and Wang, Z., 1992. Seismic properties of pore fluids. Geophysics, 57: 1396.

Best, D.L., Gardner, J.S. and Dumanoir, J.L., 1980. A computer-processed wellsite lo interpretation. SPE 9039.

Carcione, G.M., Herman, G.C. and Kroode, A.P.E. ten, 2002. Y2K Review Article, Seismic modeling. Geophysics, 67: 1304-1325.

Červený, V., 1982. Expansion of a plane wave into Gaussian beams. Studia Geophys. Geod., 26: 120-131.

Červený, V., 2001. Seismic Ray Theory. Cambridge University Press, Cambridge.

Chapman, C., 2004. Fundamentals of Seismic Wave Propagation. Cambridge University Press, Cambridge.

Christie, M.A. and Blunt, M.J., 2001. Tenth society of petroleum engineers comparative solution project: A comparison of upscaling techniques. Reservoir Simulation Symp., SPE, 72469.

Chu, C. and Stoffa, P.L., 2008. 3D acoustic wave propagations in parallel by the pseudospectral method. Expanded Abstr, 78th Ann. Internat. SEG Mtg., Las Vegas.

Clavier, C., Coates, G. and Dumanoir, J., 1984. Theoretical and experimental bases for the dual water model for interpretation of shaly sands. SPE 6859.

Dewan, J.T., 1983. Essentials of Modern Open-hole Log Interpretation. PennWell Books, Tulsa, OK.

Dvorkin, J. and Gutierrez, M., 2002. Grain sorting, porosity, and elasticity. Petrophysics, 43: 185-196.

Dvorkin, J., Mavko, G. and Gurevich, B., 2007. Fluid substitution in shaly sediments using effective porosity. Geophysics, 72: 1-8.

Galloway, W.E. and Hobday, D.K., 1996. Terrigenous Clastic Depositional Systems: Applications to Fossil Fuel and Groundwater Resources, 2nd Ed. Springer-Verlag, Berlin, Heidelberg, New York.

Gjøystdal, H., Lecomte, I., Mjelva, A.E., Maaù, F., Hùkstad, K. and Johansen, T.A., 1998. Fast repeated seismic modelling of local complex targets. Expanded Abstr., 68th Ann. Internat. SEG Mtg., New Orleans: 1452-1455.

Hill, N.R., 1990. Gaussian beam migration. Geophysics, 55: 1416-1428.

Hùkstad, K., Lecomte, I., Maaù, F.A., Tuseth, M., Mjelva, E., Gjøystdal, H.E.A. and Sollie, R., 1998. Hybrid modelling of elastic wavefield propagation. Extended Abstr., 60th EAGE Conf., Leipzig: 05-56.

Kennett, B.L.N., 1985. Seismic Wave Propagation in Stratified Media. Cambridge University Press, Cambridge.

Kirchner, A. and Shapiro, S.A., 2001. Fast repeat-modelling of time-lapse seismograms. Geophys. Prosp., 49: 557-569.

Kosloff, D.D. and Baysalt, E., 1982. Forward modeling by a Fourier method. Geophysics, 47: 1402-1412.

Lecomte, I. 1996. Hybrid modeling with ray tracing and finite difference. Expanded Abstr., 66th Ann. Internat. SEG Mtg., Denver: 699-702.

Levander, A.R., 1998. Fourth-order finite-difference P-W seismograms. Geophysics, 53: 1425-1436.

Marion, D., Nur, A., Yin, H. and Han, D., 1992. Compressional velocity and porosity in sand-clay mixtures. Geophysics, 57: 554-563.

Revil, A. and Cathles, L.M., 1999. Permeability of shaly sands. Water Resources Res., 35: 516-662.

Robertsson, J.O.A. and Chapman, C.H., 2000. An efficient method for calculating finite-difference seismograms after model alterations. Geophysics, 65: 907-918.

Shahin, A., Tatham, R.H., Stoffa, P.L. and Spikes, K.T., 2010a. Comprehensive petro-elastic modeling aimed at quantitative seismic reservoir characterization and monitoring. Poster Session, 80th Ann. Internat. SEG Mtg., Denver.

Shahin, A., Key, K., Stoffa, P.L. and Tatham, R., 2010b. Time-lapse CSEM analysis of a shaly sandstone simulated by comprehensive petro-electric modeling. Poster Session, 80th Ann. Internat. SEG Mtg., Denver.

Spikes, K., Mukerji, T., Dvorkin, J. and Mavko, G., 2007. Probabilistic seismic inversion based on rock-physics models. Geophysics, 72: 87-97.

Stoffa, P.L., Sen, M.K., Seifoullaev., R.K., Pestana, R.C. and Fokkema, J.T., 2006. Plain-wave depth migration. Geophysics, 71: 261-272.

Stoffa, P.L., Fokkema, J.T., Freire de Luna, R.M. and Kessinger, W.P., 1990. Split-step Fourier migration. Geophysics, 55: 410-421.

Tanis, M.C., Stoffa, P.L., Sen, M.K. and Fokemma, J.T., 1996. Pre-stack split-step Fourier depth migration. Extended Abstr., 58th EAGE Conf., Amsterdam: X048.

Thomas, E.C. and Stieber, S.J., 1975. The distribution of shale in sandstones and its effect upon porosity. Transactions, 16th Ann. Logging Symp., Soc. Profess. Well Log Analysts, New Orleans.

Tyler, N. and Ambrose, W.A., 1986. Facies architecture and production characteristics of strand-plain reservoirs on north Markham-North Bay City Field, Frio formation, Texas. AAPG Bull., 70: 809-829.

Uden, R., Dvorkin, J., Walls, J. and Carr, M., 2004. Lithology substitution in a sand/shale sequence. Extended Abstr., 17th ASEG Conf., Sydney.